Available online at www.sciencedirect.com
SCIENCE DIRECT®
International Journal of Heat and Mass Transfer 48 (2005) 3527–3543
International Journal of HEAT and MASS TRANSFER
www.elsevier.com/locate/ijhmt

Thermal and flow behavior of ice slurries in a vertical rectangular channel. Part I: Local distribution measurements in adiabatic flow

E. Stamatiou, M. Kawaji *

Department of Chemical Engineering and Applied Chemistry, University of Toronto, 200 College Street, Toronto, Ont., Canada M5S 3E5

Received 28 October 2004; received in revised form 25 March 2005
Available online 26 May 2005

Abstract

Local measurements of the axial mixture velocity and ice fraction profiles were conducted for the vertically, upward adiabatic ice slurry flow in a 0.305-m (W) × 0.61-m (L) × 0.025-m (gap) rectangular channel using a hot film anemometer (HFA) and an on-line ice slurry sampling/calorimetry technique. Experiments were performed at area-averaged ice fractions and mean velocities up to 16 vol% and 0.15 m s^{-1}, respectively. The ice fraction distributions systematically displayed slight peaking near the adiabatic walls for average ice fractions less than 8%; however, at higher ice fractions, the ice fraction distributions became flatter. For average ice fractions greater than 2%, the velocity distributions displayed flatter profiles than in single-phase flow, which indicates the non-Newtonian flow characteristics of ice slurries.

Keywords: Adiabatic ice slurry flow; Hot-film anemometry; Ice fraction local distributions; Velocity distributions; Non-newtonian flow characteristics

1. Introduction

Recently, there has been an increasing interest in the use of ice slurries as a phase change material for many cooling applications due to several thermo-physical and transport advantages as well as the environmentally friendly nature that ice slurries offer. Although other alternatives such as slurries of polymeric phase change materials (PCMs) and block or crushed ice have been recently developed for cooling applications (e.g., [1–3]), ice slurries are superior in many aspects due to the large latent heat and surface area density of ice crystals, as well as the dynamic behavior of ice slurry. This growing interest towards ice slurries has been demonstrated in recent years through five international workshops that have brought a large number of researchers involved in the ice slurry generation, rheology, flow and heat transfer research and some other aspects of this potential new secondary refrigerant. However, many issues are still unresolved.

Ice slurry or "slush ice" is a mixture of fine ice crystals, water and an additive such as glycol, salt or alcohol, which functions to lower the freezing point of the solution and limit the crystal size. The ice crystal sizes typically range from 0.01 mm to 1 mm in diameter depending upon the additive type and concentration

* Corresponding author. Tel.: +1 416 978 3064; fax: +1 416 978 8605.
E-mail address: kawaji@ecf.utoronto.ca (M. Kawaji).

0017-9310/$ - see front matter © 2005 Elsevier Ltd. All rights reserved.
doi:10.1016/j.ijheatmasstransfer.2005.03.020

Nomenclature

A	area, m^2
C_p	heat capacity, J kg^{-1} K^{-1}
D	diameter, m
H	channel gap, m
$\dot{H}$	heat input, W
L	length, m
$\dot{m}$	mass flow, kg s^{-1}
M	number of samples
N	number of samples
n	power law index for pseudoplastic fluids
p	power index for Newtonian fluids
Q	volumetric flow rate, m^3 s^{-1}
Re	Reynolds number
T	temperature, K
t	time, s
u	velocity or axial velocity, m s^{-1}
U_o	sampling velocity, m s^{-1}
$\langle u \rangle$	flow rate average velocity, m s^{-1}
V	integrated average velocity, m s^{-1}
W	channel width, m
X	mass fraction of solids, –
X_s	ice fraction, –
x	axial distance from inlet nozzle, m
y	transverse distance from a brass plate, m
y'	transverse distance from pipe axis, m
z	lateral distance, m

Greek symbols

α^*	aspect ratio (=channel height/width)
Δ	change in parameter
λ	latent heat of ice (=333.6 kJ kg^{-1})
μ	kinematic viscosity, Pa s
ρ	density, kg m^{-3}
Φ	ice volume fraction, vol%

Subscripts

a	antifreeze agent
b	brine or bulk
c	cross sectional
cal	calorimeter
cf	carrier fluid
crit	critical
f	final
fp	freezing (or melting) point
h	hydraulic
hy	hydrodynamic
j	instantaneous measurement
in	inlet
L	local
m	mean or average
o	sampling
out	outlet
RMS	root mean square
s	mass fraction
sl	ice slurry or solid–liquid
T	turbine
v	volume fraction
w	water

Superscripts

$'$	instantaneous component
$\cdot$	rate

[4,5] as well as the ice slurry generation method. When a freezing point depressant is not employed, ice slurry crystals larger than 1-mm in diameter are normally produced (e.g., [6]).

For the case of an adiabatic ice slurry flow, the momentum and continuity equations clearly reveal that the velocity and ice fraction distributions are coupled and interdependent [7–9]. However, often in horizontal ice slurry flows it has been observed that the ice crystals tend to accumulate near the top of the horizontal pipe at high ice fractions and low mean velocities, resulting in a considerable distortion of the velocity profile [10,11]. Alternatively, any significant change in the ice slurry velocity may alter the ice fraction distribution across the pipeline of interest.

Despite the relatively high importance of the velocity and ice fraction distributions in ice slurry flows, there has not been any known study that has attempted to quantify these distributions, which are needed to infer the form of constitutive relationships for modeling purposes. Some of the previous velocity and ice fraction distribution measurements [12–16] made in horizontal pipes or channels and in vertical ducts revealed the plug flow behavior of the ice slurries in laminar flow. However, these investigations were of preliminary nature and did not provide a systematic set of data.

Slurries of fine particle sizes are also known to exhibit non-Newtonian flow characteristics [3] due to the particle agglomeration and formation of structures. Previous investigations on the rheology of ice slurries summarized by Ayel et al. [4] have suggested that ice slurries behave as Newtonian slurries for weight ice fractions between 0 and 0.15. On the other hand, a study performed by Kitanovski and Poredos [17] suggested that the non-Newtonian flow characteristics of ice slurries not only depend on the average ice fraction but also on the mean velocity, pipe diameter and ice crystal sizes. Other factors that could also influence the rheological behavior of ice

slurries but were not treated by Kitanovski and Poredos [17] are the shape of the ice crystals, the phase densities, chemical additive type and its concentration, as well as the surface forces, which may considerably affect the ice crystal-to-crystal and carrier fluid-to-ice crystal interactions [18].

All the above-mentioned factors make it difficult to generalize the rheological behavior of ice slurries, as various researchers have employed different additive types and concentrations, and ice crystal sizes. It is thus essential to devise a viscosity measurement technique to describe the rheological properties of ice slurries and define key parameters such as the apparent viscosity needed for the definition of the Reynolds number.

Viscosity measurements for ice slurries using capillary tube viscometers, however, require significant care due to melting and stratification of the ice crystals, different gap spacing requirements depending on the carrier fluid, and the possible slip between the ice crystals and the solid wall boundaries. Thus, most of the previous investigations summarized in [4] have constructed ice slurry flow rheograms from pressure drop measurements. However, pressure drop–viscosity relation requires an assumption of a rheological model under laminar flow conditions. A direct measurement of the velocity profile overcomes this difficulty as both the flow rheogram and the flow regime may be easily identified from the velocity profiles.

The objective of the current investigation is to obtain reliable measurements of the ice fraction and velocity distributions for a vertically upward ice slurry flow in a rectangular channel and enhance our understanding of the fluid mechanical behavior of ice slurries. Some key questions that will be addressed in this paper are the following. What is the effect of the ice crystals on the velocity profile? For a specified ice fraction, what is the effect of the mean velocity or Reynolds number on the ice slurry velocity distribution? For what ice fraction ranges and bulk velocities can the ice slurry be treated as a Newtonian fluid?

To further facilitate this study, the ice slurry experiments were performed in a vertical channel to eliminate the gravitational effects that cause phase separation phenomena encountered in horizontal channels. In vertical flows, the ice fraction distribution should be reasonably symmetric about the channel axis [9]. To reduce measurement uncertainty and avoid possible damages to the hot film probe, experiments were restricted to flow conditions where the area-averaged ice fraction and mean axial velocity were less than 9% (by volume) and 0.15 m s^{-1}, respectively. Although the latter seems to be at first glance somewhat low, the range tested would be typical of ice slurry velocities encountered in compact plate heat exchangers consisting of multiple plates. On the other hand, local ice fraction measurements were made for average volume ice fractions up to 16%. The corresponding Reynolds numbers investigated based on the liquid properties and hydraulic diameter ranged from 2100 to 4200.

2. Experimental details

2.1. Working fluid

An ice slurry mixture was generated in a hypoeutectic solution of 6.2% by weight NaCl in water (brine) with a corresponding freezing point temperature of −3.75 °C. Fig. 1 is a sample photograph of the ice crystals used in the current study. A 500-μm diameter needle is immersed in the ice slurry sample to illustrate the approximate size of the ice crystals. Several images that were analyzed using image analysis software indicated that the mean ice crystal sizes ranged from 100 to 200 μm. Also, the ice crystals did not appreciably agglomerate or coalesce over the 6-h duration of each experiment.

2.2. Experimental apparatus

The experimental apparatus is shown schematically in Fig. 2. The major components were: a 450-l capacity well-insulated storage tank; a variable speed centrifugal pump (Eastern, Model: Centrichem); a rectangular test section with hydrodynamic entry, main and exit sections; and a 12-kW refrigeration capacity ice slurry generator (Sunwell, Model: Deepchill™ IG-6VM) that was used to produce and control the ice fraction at the test section inlet. The ice slurry volumetric flow rate was measured using an electromagnetic flow meter

Fig. 1. Typical ice slurry crystals compared with a 500-μm diameter needle.

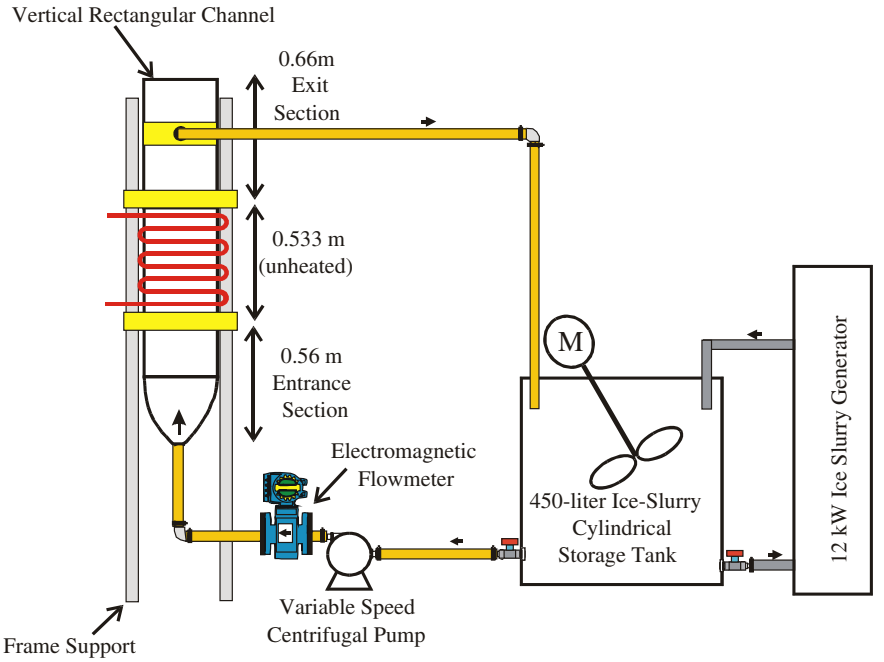

Fig. 2. Schematic diagram of flow loop for the adiabatic ice slurry flow.

(Endress+Hauser, Promag 30) that was calibrated at different ice fractions and ice slurry flow rates with an accuracy of ±0.50%.

To maintain a uniform ice fraction in the 450-l reservoir, a 250-W variable speed mixer (Leeson, Model: E2V) was installed on top of the tank. In addition to the mechanical mixing, tangential inlets from the ice generator and rectangular channel were employed to generate a large enough vortex in the mixing tank and thus provide good mixing of ice crystals in the ice slurry. The inlet piping connections to the vertical test section were made of 25.4-mm ID flexible braided tubing and PVC schedule 80 pipes to ensure that a high enough velocity is maintained and a homogeneous ice slurry flow enters the test section. On the other hand, the test section outlet consisted of flexible braided hose of sufficiently large diameter (a 76.2-mm ID) to prevent the ice slurry from plugging it.

Fig. 3 gives the details of the rectangular test section, which could also be used as a heat exchanger to heat the ice slurry. The main flow section consisted of a custom-made rectangular transparent flow channel that was 0.31-m wide and 0.61-m long. A 25.4-mm flow channel gap was formed between a vertical brass plate (0.36 m $(W) \times 0.61$ m $(H) \times 19$-mm thickness) and a 25.4-mm thick acrylic plate, through which the ice slurry was recirculated vertically upward. The corresponding channel gap to width aspect ratio, α^*, was 1:12. The hydraulic diameter, D_h, defined as $4 \times$ cross sectional area over the wetted perimeter was 0.047 m.

The rectangular flow channel was connected to entrance and exit transition sections, which were 0.56 and 0.66 m long, respectively, and had similar rectangular cross sections as the main flow chamber. The inlet hydrodynamic transition section contained flow straighteners and many equally spaced circular rods to obtain a uniform inlet flow. The use of transparent acrylic plates to construct the test section allowed for visual inspections of the ice slurry flow inside the rectangular channel. In the current work, the side and front acrylic walls were maintained at nearly adiabatic conditions. The back of the brass plate, the inlet and outlet piping connections to the test section and storage tank were all covered with a Rubatex® thermal insulation to minimize any heat gains from the surroundings.

2.3. Measurement techniques and instrumentation

2.3.1. On-line ice fraction measurement technique

Local ice fraction distribution measurements were made by continuously removing an ice slurry sample using a 5.84-mm ID, L-shaped stainless steel tube (0.51-mm wall thickness). The sampling probe was inserted into the main flow through an opening in the acrylic channel wall (see Fig. 4(a)). The sampling tube's opening was slightly enlarged (7.6-mm ID) and sharpened to allow for the easy passage of ice crystals as recommended by Nasr-El-Din et al. [19].

The ice slurry sampling tube was traversed and positioned at three selected locations across the flow channel

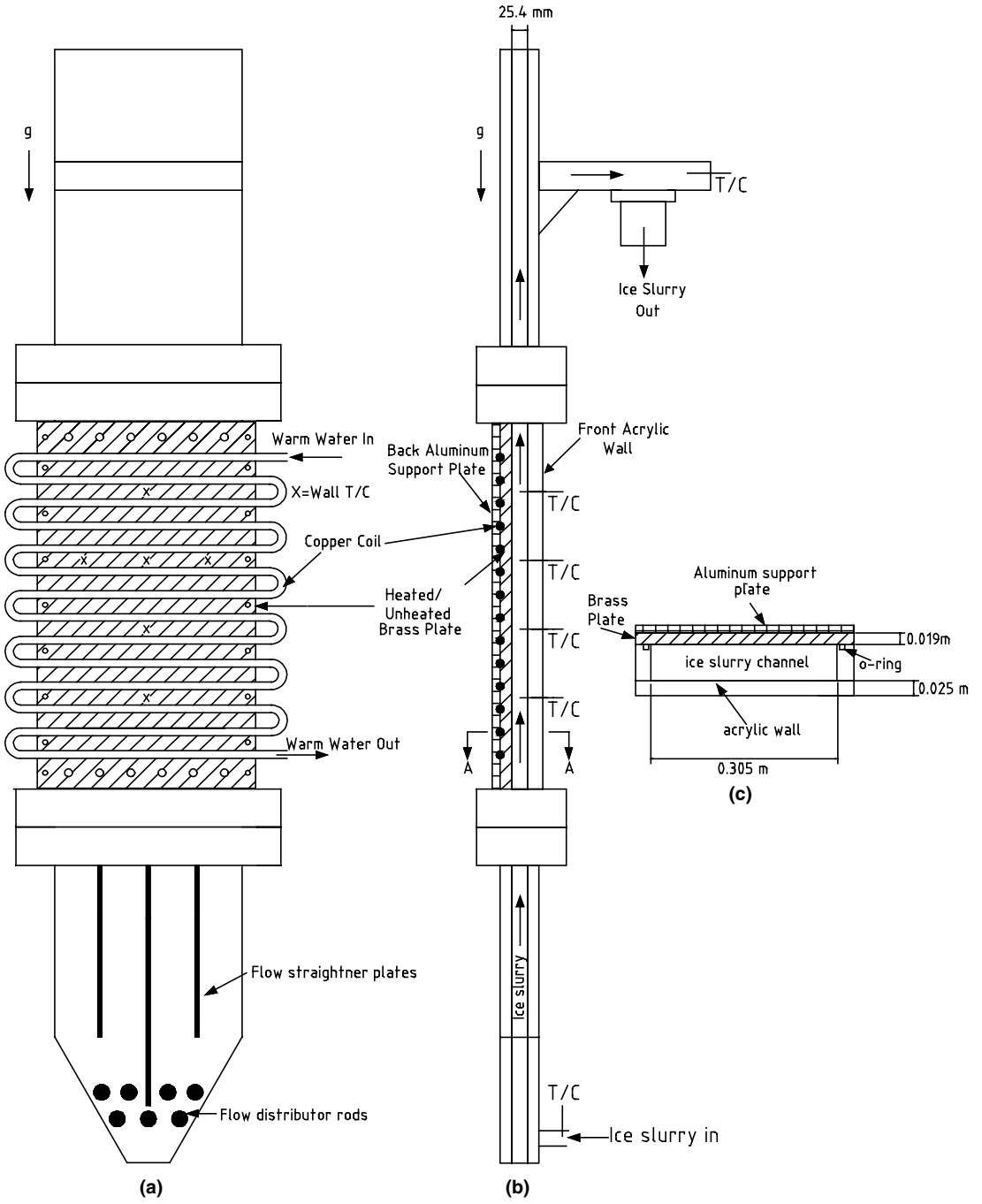

Fig. 3. Cross sectional views of the rectangular channel/heat exchanger: (a) rear view, (b) side view, and (c) cross sectional view (A–A).

between the vertical brass plate and front acrylic wall (see Fig. 4(a)). The traversible sampling tube was installed mid-width through the flow channel ($z/W = 0.50$) at the axial location of $x/D_h \sim 19$, where x is the distance measured from the inlet nozzle. At steady state, the ice slurry sample at a selected sampling position was diverted to the custom-made on-line calorimeter unit that was instrumented and properly calibrated (see Fig. 4(b)). The heated section of the on-line calorimeter was long enough ($L \sim 5$) to ensure complete melting of the ice crystals. The local ice fraction content was determined from a heat balance as described later. A sampling period of approximately 30 or 60 s was chosen for each local ice fraction measurement. The signals

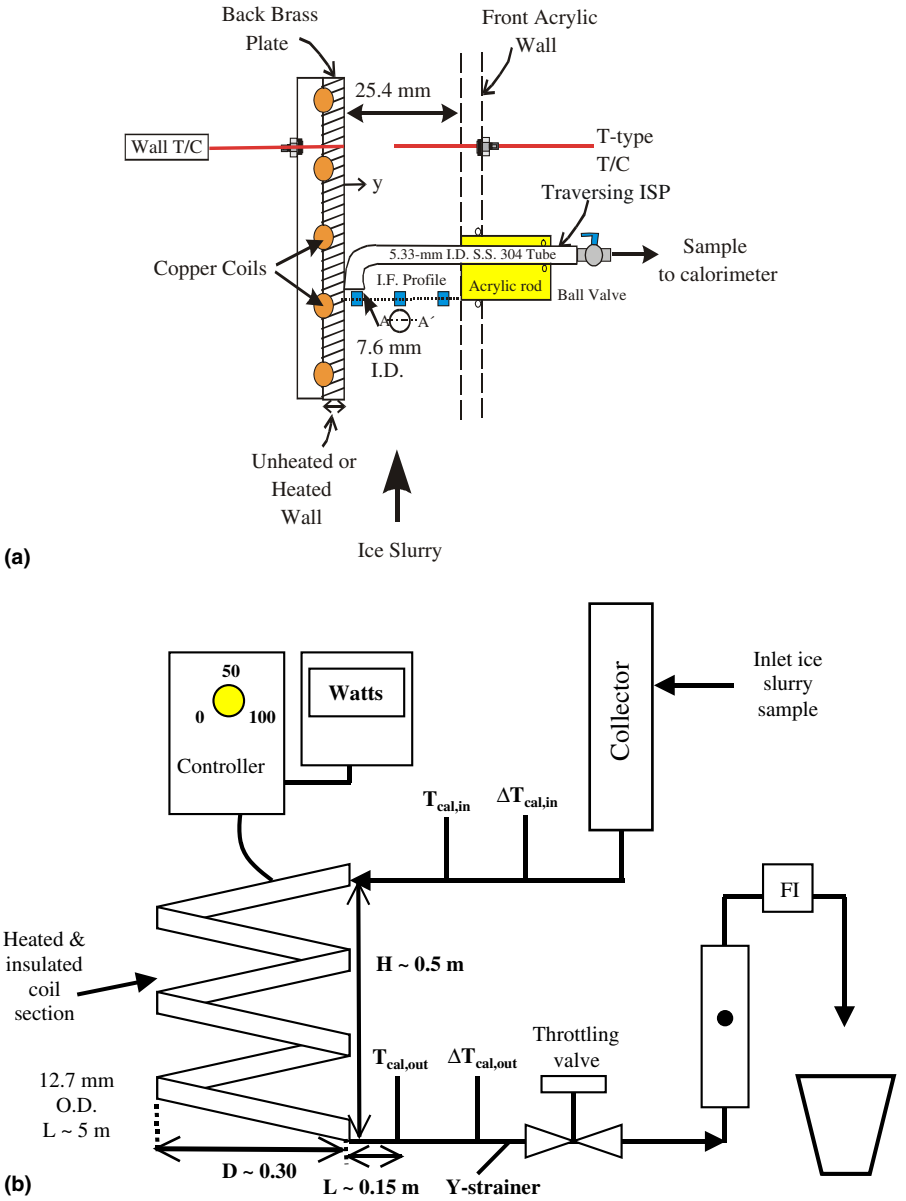

Fig. 4. Local ice fraction measurement system (a) ice slurry sampling probe (ISP) (side view), and (b) on-line calorimeter (680-W).

from the various calorimeter instruments were measured using a PC-based data acquisition system (National Instruments, PC-MIO-16-E4) with a signal-conditioning unit (National Instruments, SCXI-1000) that was controlled by Labview 5.1 data acquisition software. A sampling rate of 1 Hz was adopted for recording the steady state readings.

2.3.2. Ice slurry velocity measurements

Mean axial velocity measurements were made using a 90° cross flow, miniature conical hot film probe (TSI, Model: 1231AR), which was mounted on a probe support (TSI, Model: 1150-6). The hot film-sensing element was composed of a high purity platinum film with a fused-quartz substrate coating for providing anticorrosive properties, high strength and low thermal conductivity. This hot film probe had a sensing element diameter of 127 μm, and a corresponding sensing length of 1.02 mm, which gave a good spatial resolution. After removing the ice slurry sampling probe, the hot film probe was installed mid-width ($z/W = 0.50$) through the rectangular flow channel at the axial location of

$x/D_h \sim 20$ (or $x = 0.92$ m) from the inlet nozzle. The probe was manually traversed to measure mean velocity at seven selected positions across the flow channel using a slide-potentiometer as shown in Fig. 5.

The output voltage signal from the hot film probe was connected to a constant temperature anemometer (CTA) bridge (Dantec, Model: 56C17). In the CTA anemometer, the cooling effect produced by the flow passing over the sensing element was balanced by the electrical current supplied by the anemometer, so that the hot film element would be maintained at a constant temperature. Any changes in the velocity would thus show up as a change in the anemometer output voltage. Since the principle of the thermal anemometry is to measure the fluid velocity by sensing any changes in the heat transfer rate between the sensor element and its environment, the anemometer will also respond to any changes in parameters other than the velocity, such as the temperature and composition of the ice slurry mixture. To account for this, the anemometer's output voltage was calibrated over different desired ice fraction and velocity ranges using a rotating pool of ice slurry in a 30 cm-diameter circular container placed on a turntable. The results of this calibration are given elsewhere [20].

From the calibration data, the anemometer's output voltage was seen to increase with both the velocity and ice fraction [20]. However, due a small effect of the ice fraction on the anemometer's output voltage for a given velocity, a single polynomial curve was fitted to represent the entire range of non-zero ice fraction data for different velocities (X_s = 2–12%). Another calibration curve was fitted to the zero ice fraction results for different velocities (X_s = 0.0%). The small difference between the finite and zero ice fraction calibration data was attributed mostly to the different fluid temperatures at which the data were collected rather than the ice fraction content as the fluid temperature is known to affect the hot film anemometer measurements [21].

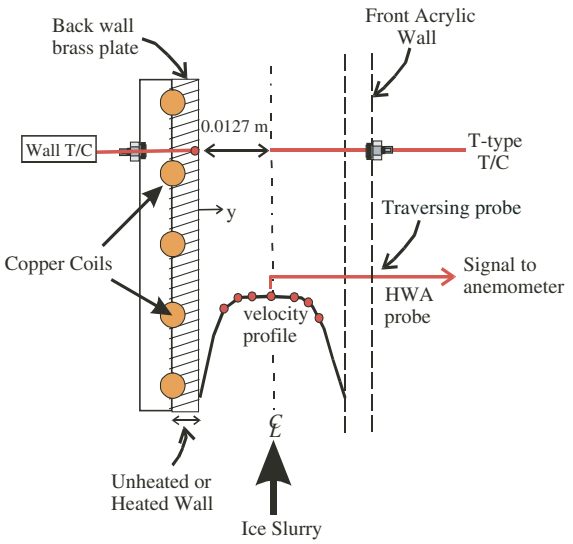

Fig. 5. Local velocity measurement (side view) using a hot film anemometer probe.

The uncertainty in the hot film measurements could arise due to slight misalignment of the probe with respect to the ice slurry flow direction. This was addressed by purposely changing the orientation of the hot film probe by 2° angle from the flow direction during a bench scale calibration test and recording the difference in the anemometer voltage data. The maximum uncertainty in the hot-film calibration data was 5% or 0.60 cm/s.

For the adiabatic and diabatic ice slurry flow measurements, the calibration curves were used to determine the local ice slurry velocity profile across the rectangular flow channel. The steady state anemometer output voltages were collected at a sampling rate of 5 Hz using Labview 5.1 and a PC data acquisition system, as described previously.

2.4. Test procedure

Experiments were performed by first producing an ice slurry in a storage tank containing a hypoeutectic solution of 6.2% by weight NaCl in water (brine) using a 12-kW scraped-surface ice slurry generator (see Fig. 2). During the tests, the ice slurry generator (IG) was left on and its temperature controller was periodically adjusted to vary the ice slurry production rate and maintain a desired ice fraction at the inlet of the test section. The ice slurry was circulated from the storage tank vertically upward through the test section using a variable speed centrifugal pump. During the adiabatic tests, about 2–3 kg of ice slurry samples were withdrawn from the inlet and outlet of the test section. An average of the two ice fractions is reported for all the experimental runs, which is denoted as Φ_v (volume ice fraction) or X_s (mass ice fraction). The ice fraction was determined using a batch calorimetric method. The absolute uncertainty in these batch ice fraction measurements was ±1%. Adiabatic ice fraction and velocity distribution measurements were made during the steady state operation, as established by minimal changes in the ice slurry flow rate, average ice fraction, and temperatures recorded using various thermocouples installed in the rectangular test channel.

3. Data reduction

3.1. Local and mean ice fraction

The local ice fraction at a particular transverse location, y, was calculated by statistical averaging,

$$X_s(y) = \frac{1}{M}\sum_{i=1}^{M} X_{s,i}(y,t) \tag{1}$$

where $X_{s,i}(y,t)$ refers to the ith instantaneous ice fraction reading at the location y, and M is the total number of data points obtained at the y location. For each location y, at least 30 local instantaneous ice fraction readings collected over a 30-s time interval were timed-averaged. The instantaneous ice fraction, $X_{s,i}(y,t)$ was evaluated from a heat balance performed across the on-line calorimeter, i.e.,

$$\dot{H}_i(y,t) = \dot{m}_T\left\{X_{s,i}(y,t)\lambda_{ice} + \int_{T_{sl}}^{T_f}(1 - X_{s,i}(y,t))c_{p,a}\,dT + \int_{T_{sl}}^{T_{fp}}(X_{s,i}(y,t))c_{p,ice}\,dT + \int_{T_{fp}}^{T_f} X_{s,i}(y,t)c_{p,w}\,dT\right\} \tag{2}$$

where $\dot{H}_i(y,t)$ is the instantaneous heat input (Watts) measured using a calibrated power meter, $\dot{m}_T$ is the instantaneous mass flow rate (kg s^{-1}) measured at the exit of the on-line calorimeter using a calibrated turbine flow meter, λ_{ice} is the latent heat of fusion of ice (333.6 kJ kg^{-1}), $c_{p,a}$ (~3.85 kJ kg^{-1} K), $c_{p,ice}$ (~2.1 kJ kg^{-1} K) and $c_{p,w}$ (~4.2 kJ kg^{-1} K) are the specific heat capacities of the carrier fluid (NaCl–water), ice and pure water, respectively, and T_f, T_{sl}, T_{fp} (K) refer to the exit, inlet and freezing point temperatures of the ice slurry sample, respectively. In Eq. (2), the heat of mixing of water and NaCl was neglected as the sensible and latent heat terms are much greater than that of heat of mixing.

All local ice fraction measurements were made by maintaining the heat input to the calorimeter constant at 100%. The on-line calorimeter flow rate was adjusted by throttling the exit valve such that T_f was always greater than 0 °C by a few degrees to ensure complete melting of all ice crystals. The on-line calorimeter was calibrated by varying the flow rate and heat input for a single-phase liquid flow ($T_b > T_{fp} \sim -3.0$ °C) and measuring the accompanying temperature rise across the calorimeter [20]. The temperature sensors in the on-line calorimeter were also calibrated by passing a brine stream through the on-line calorimeter (at $T_b = -3.0$ °C) without adding any heat and correcting for any temperature discrepancies in the readings. Finally, the on-line turbine flow meter was also calibrated by measuring the mass flow rate at the exit of the calorimeter using a container and a stopwatch.

3.2. Local and mean ice slurry velocity

The local axial ice slurry velocity was computed as follows:

$$u(y) = \frac{1}{N}\sum_{j=1}^{N} u_j(y,t) \tag{3}$$

where $u_j(y,t)$ is the jth instantaneous ice slurry velocity at the transverse location, y, and N is the total number of data points for the y location. For each location y, at least 100 instantaneous local velocity readings (u_j) were time-averaged and collected over a time period of 20 s.

For the case of ice slurry flow, the HFA system responds differently to the ice crystals in the ice slurry and the brine due to the dramatic differences in the thermal properties between the two phases. This can lead to an abrupt change in the anemometer's output signal when the hot-film element encounters an ice crystal, which is similar to that experienced in air–water flows [22]. In this investigation, it is assumed that the hot-film probe signal yields the mixture ice slurry velocity since the local slip velocity is very small (~1.6×10^{-3} m s^{-1}) compared to the local ice slurry velocity.

The accuracy of the mean axial ice slurry mixture velocity was checked by comparing the area-averaged mixture velocity, V, to the corresponding inlet ice slurry volumetric flux given by the electromagnetic flow meter Q_{sl} as,

$$\langle u_{sl}\rangle = Q_{sl}/A \tag{4}$$

3.3. Flow parameters

Two definitions of the Reynolds number were adopted in the current investigation. The first definition, Re_{cf}, was based on the liquid properties (carrier fluid),

$$Re_{cf} = \frac{\rho_{cf}\langle u_{sl}\rangle D_h}{\mu_{cf}} \tag{5}$$

where ρ and μ are the density and viscosity, respectively, $\langle u_{sl}\rangle$ is the mean axial velocity obtained from the cross sectional average volumetric flow rate, D_h is the hydraulic diameter, and the subscript cf refers to the carrier fluid (brine).

The second Reynolds number definition, Re_{sl}, was evaluated based on the ice slurry mixture properties assuming homogeneous ice slurry flow,

$$Re_{sl} = \frac{\rho_{sl}\langle u_{sl}\rangle D_h}{\mu_{sl}} \tag{6}$$

The ice slurry density ρ_{sl} was expressed in terms of component densities and was computed using the following equation, as suggested by Wasp et al. [23] and Guilpart et al. [24] among others,

$$\rho_{sl} = \frac{1}{\frac{X_s}{\rho_{ice}} + \frac{1 - X_s}{\rho_{cf}}} \tag{7}$$

In Eq. (7), X_s is the weight fraction of ice, and ρ_{cf} is the density of the carrier fluid evaluated at the specified ice slurry temperature and initial salt concentration. The ice slurry viscosity in Eq. (6) was estimated using the

viscosity model proposed by Thomas [25] and used by others [5,24].

3.4. Benchmark tests in single-phase liquid flow

To check the validity of the hot film measurements, single-phase velocity distribution measurements were made for the brine flow at $Re_{cf}(=\rho\langle u_b\rangle D_h/\mu)\sim 2200$ and at a mean liquid temperature of −3.5 °C ($T_b > T_{fp}$). Fig. 6 compares the HFA data with those predicted by an empirical formula for the turbulent flow in circular ducts that may be applied to rectangular channels and $Re_{cf} > 2100$ [22,26]:

$$\frac{u(y')}{V}=\frac{(p+1)(2p+1)}{2p^2}\left(1-\frac{2y'}{H}\right)^{1/p};\quad p=2.95Re_{cf}^{0.0805} \tag{8}$$

The velocity profile for a laminar flow in a rectangular duct and that predicted by a computational fluid dynamics (CFD) code PHOENICS for turbulent flow between parallel plates are also compared in this figure. An approximate velocity profile solution for the fully developed laminar flow of Newtonian fluids in rectangular ducts is given in Ref. [26]. In this figure the error bars were estimated from the sum of the least squares of uncertainties in the calibration curve. Also in Fig. 6 and hereafter, each velocity point represents the time-averaged velocity of about 100 instantaneous local velocity readings (u_j) at each transverse location, y, made over a period of 20 s during steady flow.

As shown in Fig. 6, a fair agreement was found among the HFA data, the predictions of empirical equations and the PHOENICS code with a k–ε model for turbulent flow between parallel plates with a uniform inlet velocity of 0.105 m s^{-1}, except at the location of $y/H\sim 0.33$. For that location, the two sets of independent experiments conducted with two different hot-film probes showed a spike in the velocity data that could not be predicted by the PHOENICS code, but can be better approximated by the laminar flow in a rectangular duct.

The discrepancy between the average velocity, $V = 0.105$ m s^{-1}, obtained by integrating the measured velocity profile shown in Fig. 6 and the flow rate based average velocity, $\langle u_b\rangle = 0.082$ m s^{-1}, is attributed to the higher centerline ($z/W = 0.50$) velocity compared to the average over the entire width. The higher centerline average velocity may be a result of several factors such as the location of the inlet, the inlet duct geometry, and three-dimensional effects that could affect the uniformity of the flow. A preliminary 3-D PHOENICS code simulation also performed for a rectangular channel showed that the current flow situation had a higher centerline velocity than the mean velocity over the lateral width.

The velocity profile in Fig. 6 indicates that the flow is turbulent at $Re_{cf}\sim 2180$. For flow in rectangular ducts, the entrance configuration and channel aspect ratio have been shown to exert a marked influence on the critical Reynolds number, and Re_{crit} could vary from 2200 to

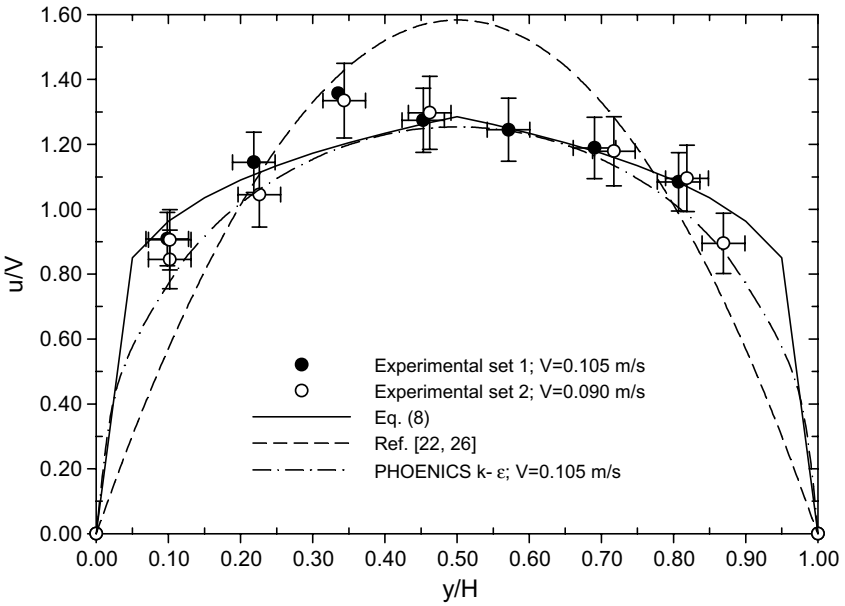

Fig. 6. Single-phase velocity profile using HFA at $x/D_h\sim 20$. $\Phi_v = 0.0\%$, $T_b = -3.5$ °C, $Q_b = 38.3$ l/min, $Re_{cf} = 2180$, $V = 0.105$ m s^{-1}, $\langle u_b\rangle = 0.082$ m s^{-1}.

6000 [27]. Thus, the velocity profile is the best method of identifying the flow regime as the present inlet configuration is rather complex. Bhatti and Shah [27] have used the criterion of $Re_{cf} > 2000$ for turbulent flow in non-circular ducts, which is also in agreement with the current results.

The hydrodynamic entry length, L_{hy} required for fully developed turbulent flow in a circular tube is given by Bhatti and Shah [27],

$$L_{hy}/D_h = 1.3590 Re_{cf}^{0.25} \tag{9}$$

Using Eq. (10), an axial distance of about 10 hydraulic diameters is required to obtain fully developed conditions flow at $Re_{cf} = 2200$, which suggests that the current single-phase flow is fully developed, as the entrance length to the measurement station was approximately 20 hydraulic diameters ($x \sim 0.92$ m).

4. Results and discussion

4.1. Adiabatic ice slurry velocity distribution

Local ice slurry velocity profiles were measured at mean bulk velocities of ~0.10 and 0.15 m s^{-1}, and volume ice fractions (Φ_v) of up to ~10%. The data are presented in Figs. 7 and 8, and the effects of ice fraction and Reynolds number are discussed below.

4.1.1. Effect of ice fraction

Fig. 7(a) compares the velocity distributions obtained for extremely low volume ice fractions ($\Phi_v < 1\%$) with that for single-phase flow at the bulk velocity of 0.080 m s^{-1}. This figure also shows the velocity profiles given by an empirical formula, Eq. (8), and predicted by PHOENICS for turbulent flow between parallel plates. At these very low ice fractions, the ice crystals do not have a significant effect on the velocity profile and the ice slurry behaves in the same manner as a single-phase flow.

Fig. 7(b) shows the effect of ice fraction on the ice slurry velocity distribution for runs conducted at the same mean axial velocity of 0.080 m s^{-1} but different volume ice fractions, $\Phi_v = 0\%$ (single-phase) to 6%. In this figure the error bars are omitted for clarity, but are similar in magnitude to those in Fig. 7(a). From Fig. 7(b), it is evident that the ice crystals have an effect of producing a blunt velocity profile that deviates significantly from the profile measured in a single-phase flow. As the volume ice fraction increases the velocity profile becomes flatter since the mixture Reynolds number, Re_{sl}, is reduced due to an increase in the apparent viscosity ($\mu_{cf} = 1.85$cp at $\Phi_v = 0.0\%$ to $\mu_{sl} = 2.2$cp at $\Phi_v = 6\%$). This suggests that the ice slurry flow may become relaminarized with increasing ice fraction since the HFA velocity data could be predicted by a laminar non-Newtonian velocity profile as discussed next.

Fig. 7(b) also compares the laminar velocity profile for a non-Newtonian flow between two infinitely long parallel plates given by Eq. (10) [26],

$$\frac{u(y')}{V} = \frac{2n+1}{n+1}\left[1 - \left(\frac{2y'}{H}\right)^{n+1/n}\right] \tag{10}$$

where n is the power law index and y' is the transverse rectilinear coordinate measured from the mid-plane of the flow channel. Most of the ice slurry HFA results presented in Figs. 7(b) and 8 were best predicted when the power law index n had a value of 0.25, while the PHOENICS code with Thomas's viscosity correlation failed to predict the present HFA measurements. The power law index of 0.25 suggests that ice slurry may be treated as a pseudoplastic fluid, which is similar to the behavior reported by Ben-Lakhdar et al. [28] based on ice slurry pressure drop measurements.

As Figs. 7(b) and 8 also illustrate, this power law index n may predict the velocity profiles for the volume ice fraction of 2–9%, except at $y/H \sim 0.10$. Despite the fact that other researchers have also interpreted their ice slurries as Bingham plastic or Casson fluid from pressure drop measurements [4], only the power law model was attempted to fit the present ice slurry velocity profile data as it is the most widely used and simplest model to apply and adequately describes the present HFA profiles. In the present investigation, however, the non-Newtonian flow characteristics of ice slurries were detected at much lower ice fractions ($\Phi_v \geqslant 2\%$) since the hot-film anemometer is a much more sensitive instrument than the conventional pressure-drop measurements.

Earlier investigations into the influence of solid particles on the velocity profile have suggested the migration of the particles to a low shear region towards the center of the pipe that result in blunt velocity profiles (e.g., [29–31]). However, Matas et al. [32] and Hampton et al. [33] recently pointed out that the velocity blunting effect due to the particle migration alone becomes only important at small Reynolds numbers ($Re < 700$), high particle concentrations ($\Phi_v > 25\%$), and when the ratio of the pipe diameter to the particle diameter, D_h/d_s, is small (typically <65), i.e., conditions that are more likely to occur in capillary tube viscometers. The present velocity profiles presented in Figs. 7 and 8 were obtained at an ice fraction of $\Phi_v < 10\%$ and a ratio of $D_h/d_s \sim 300$, thus the inward migration of ice particles towards the channel axis is highly unlikely to occur under these experimental conditions.

4.1.2. Effect of Reynolds number

Fig. 8 shows the effect of Reynolds number on the velocity profile for volume ice fractions of 2.0%, 6%

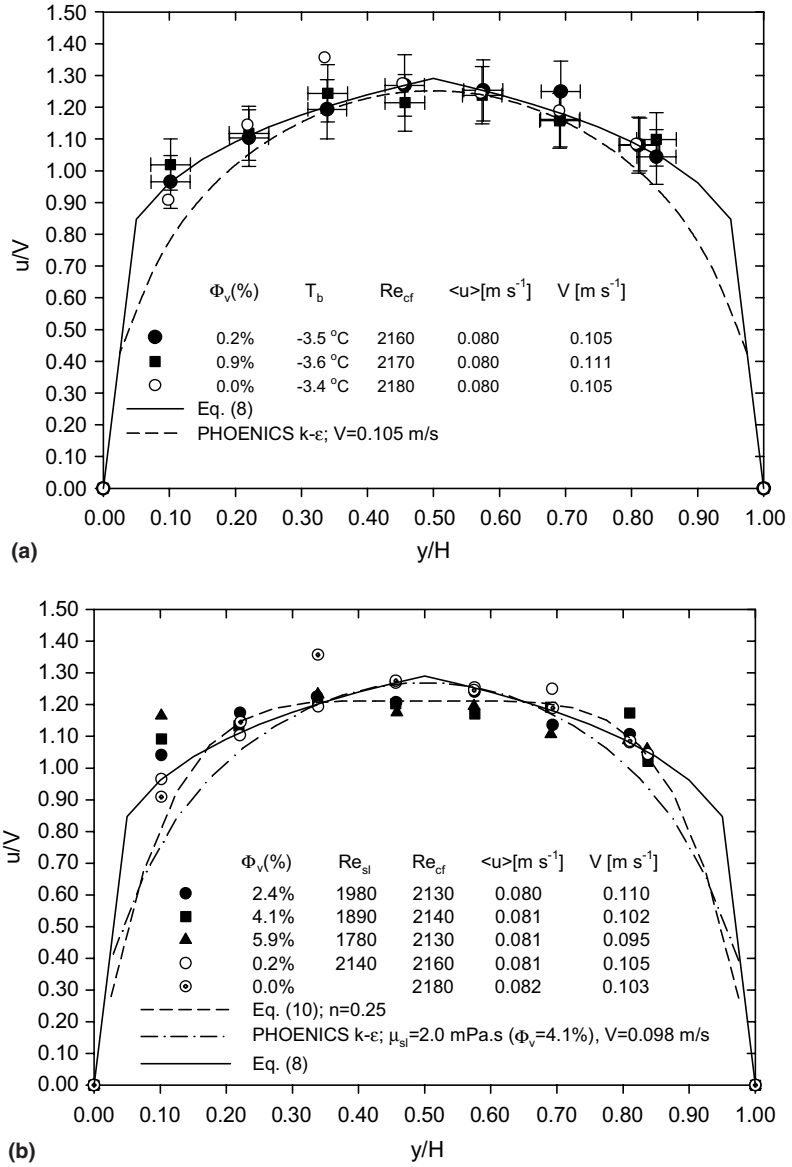

Fig. 7. Adiabatic velocity profiles for (a) $\Phi_v < 1\%$ and $\langle u_{sl}\rangle = 0.080$ m s^{-1}, and (b) $\Phi_v \sim 0.0$–6.0% and $\langle u_{sl}\rangle = 0.080$ m s^{-1}.

and 9%. Both Fig. 8(a) and (b) suggest that there is no change in the ice slurry velocity distributions when the Reynolds number (Re_{cf}) is increased from ~2100 to 4000. Fig. 8(a) and (b) also show a better agreement between the profile-averaged velocities, V, and flow rate-based average velocities, $\langle u\rangle$, for the higher Reynolds number cases, which may be due to the lower uncertainty in the velocity measurement at the higher ice slurry velocities and the flatter velocity profiles incurred for these runs. The flatter velocity profiles also meant reduced velocity peaking at the centerline ($z/W = 0$) that was previously suggested to occur in the single-phase flow runs.

In this investigation, the non-Newtonian flow characteristics of ice slurry flows cannot be generally limited to high ice fractions as previously reported by Ayel et al. [4], since the present velocity profile data for low ice fractions ($\Phi_v = 2$–9%) show flatter profiles than the single-phase flows.

4.2. Ice slurry transitional flow

The non-Newtonian flow characteristics that ice slurries display could affect the value of the critical Reynolds number, Re_{crit}. The critical Reynolds number for time-independent power law fluids depends upon the type

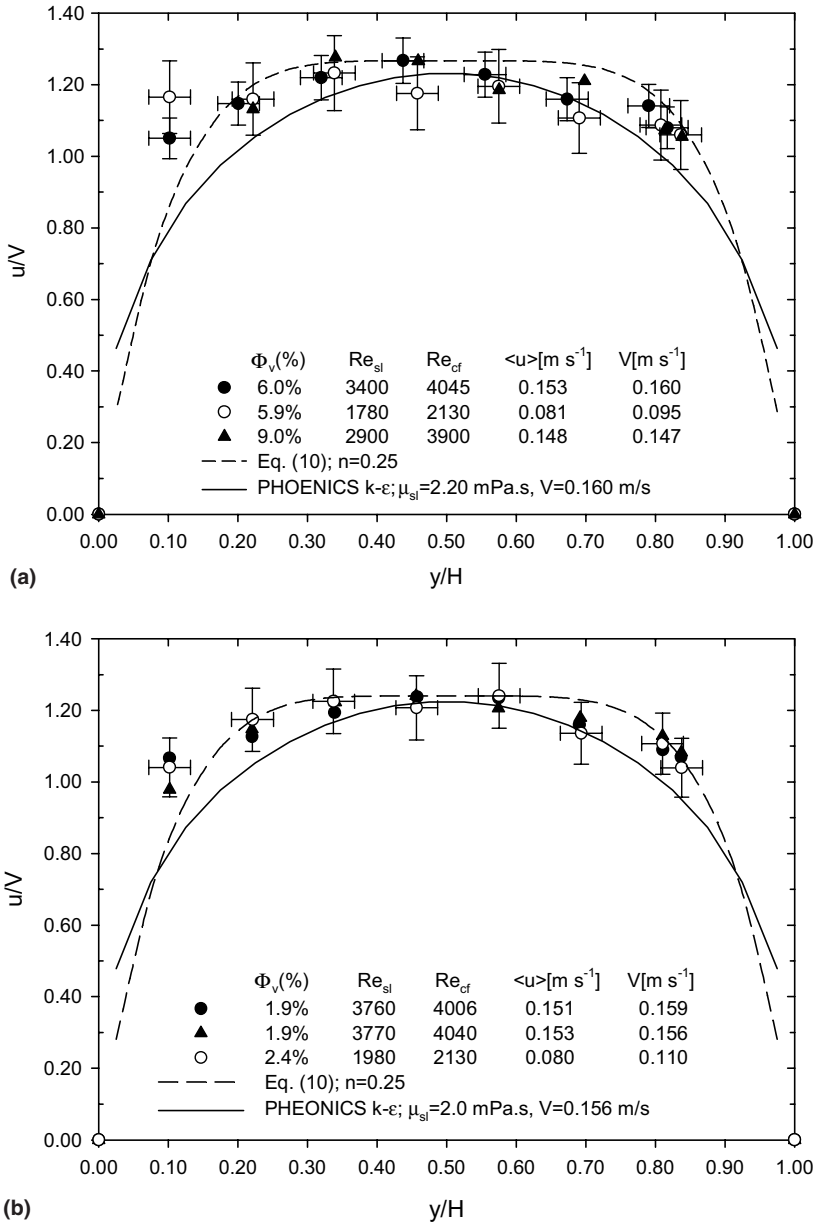

Fig. 8. Effect of Reynolds number on the ice slurry velocity distribution for (a) $\Phi_v \sim 6.0$–9.0% and (b) $\Phi_v \sim 2\%$.

and degree of non-Newtonian behavior. In the absence of any definite measure of the critical Reynolds number for the non-Newtonian ice slurry flow in rectangular ducts, the velocity fluctuations of the hot-film anemometer signal were analyzed to establish the transition from laminar to turbulent flow. It is argued that the velocity fluctuations in turbulent flow should be considerably higher than in the corresponding laminar or transitional flow cases for similar ice fraction ranges.

The streamwise ice slurry turbulence intensities were evaluated as the root-mean-square of the ice slurry velocity data, $u_{\mathrm{RMS}} = \sqrt{\overline{(u'^2)}}$. In this calculation, the velocity fluctuation component, u', was first computed as the deviation of the instantaneous streamwise velocity, u_j, from the time-averaged velocity, $\langle u_m \rangle$, using about 100 instantaneous velocity data ($u' = u_j - \langle u_m \rangle$) at each location, y. Then, the variances $\overline{(u'^2)}$ of the instantaneous values were computed from the mean, and finally the square root was taken. For each transverse location, y/H, about 100 instantaneous velocity data (u_j) were collected at a sampling rate of 5 Hz over a period of 20 s. The results of this analysis are shown in Fig. 9(a)–(c).

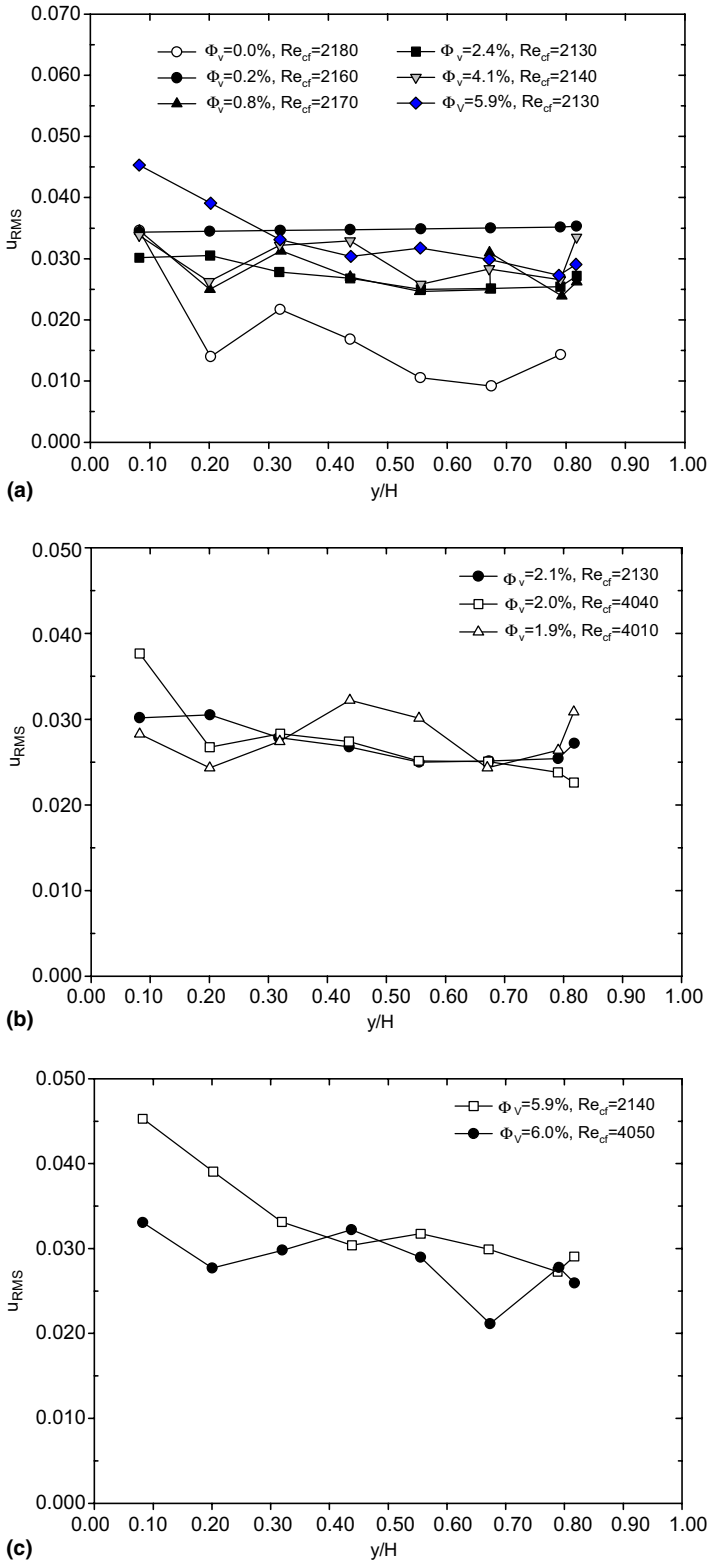

Fig. 9. Turbulence intensities for (a) different Φ_v and $Re_{cf} \sim 2200$, (b) different Re_{cf} and $\Phi_v \sim 2\%$, and (c) different Re_{cf} and $\Phi_v \sim 6\%$.

Fig. 9(a) compares the RMS velocity fluctuations at different ice fractions and transverse positions across the rectangular channel for $Re_{cf} \sim 2200$. The velocity fluctuations at the same Reynolds number increased in comparison to single-phase brine flow due to the presence of ice crystals, which are constantly hitting the hot film probe. However, there is no systematic trend in RMS values with increasing ice fraction perhaps due to the small ice fraction ranges studied.

Fig. 9(b) compares the RMS velocity fluctuations at two different Reynolds numbers (~2200 and 4000) at an average ice fraction of $\Phi_v \sim 2\%$. This figure suggests that the RMS value does not increase with increasing Reynolds number for similar ice fractions. This is also shown in Fig. 9(c) for an average ice fraction of $\Phi_v \sim 6\%$. Since the turbulent velocity fluctuations do not appreciably increase when the Reynolds number is increased from 2200 to 4000, and the corresponding

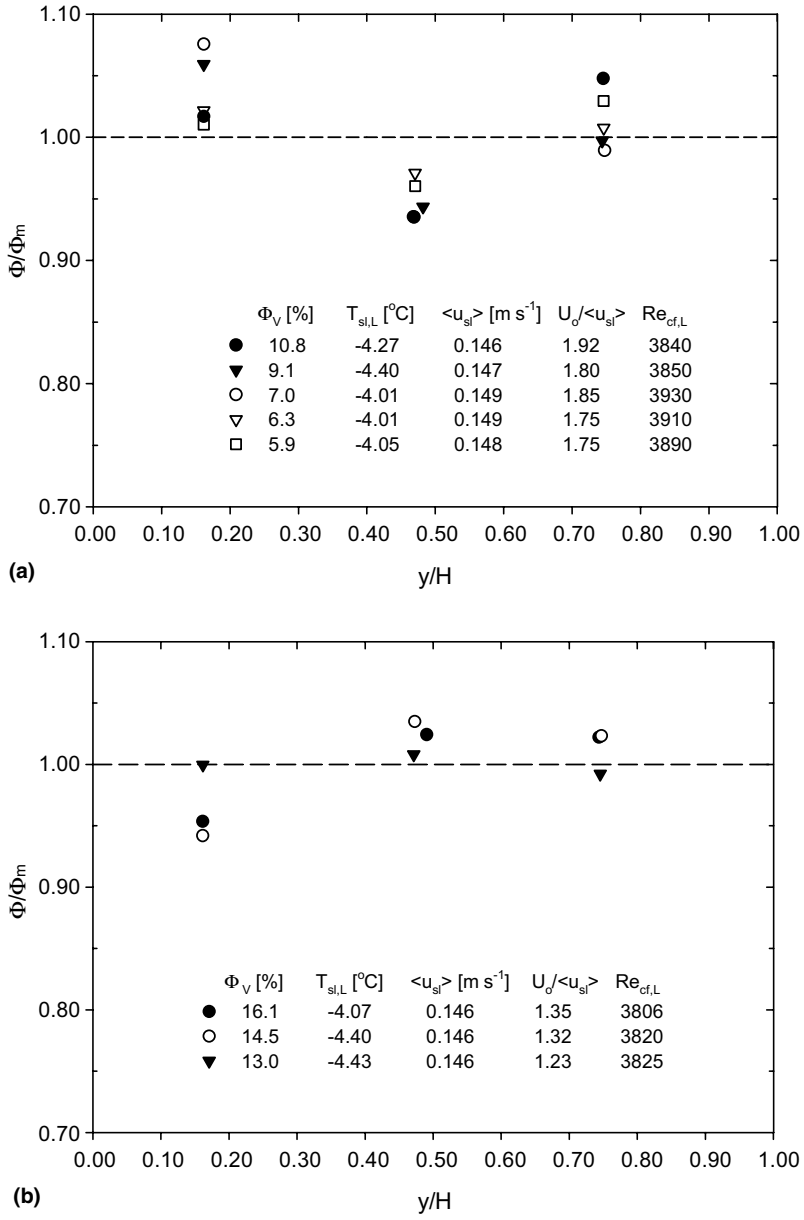

Fig. 10. Ice fraction distributions for (a) Φ_v (6–11%), $U_o/\langle u_{sl}\rangle \sim 1.8$ and (b) $\Phi_v > 13\%$, $U_o/\langle u_{sl}\rangle \sim 1.3$.

HFA velocity data presented in Figs. 7(b) and 8 could be predicted by a laminar non-Newtonian flow model, Eq. (10), the ice slurry flow is judged to retain its laminar character over the present Reynolds number range. The laminar flow at extended Reynolds numbers can be attributed to the ice crystals present in the ice slurry, which increase the mixture viscosity and thus re-laminarize the flow. The delay in the transition to higher Re_{crit} due to the enhanced apparent viscosity caused by the ice crystals was also reported by Matas et al. [32] in experiments with polystyrene particles of $d_s = 40$–780 μm suspended in a glycerol/water solution at $\Phi_v = 5$–25%.

4.3. Ice fraction distributions

The effect of ice slurry sampling velocity (U_o) was first studied to examine the measurement errors when the ice slurry sample is not withdrawn isokinetically [19]. Although not shown here, there were no major systematic errors detected in the local ice fraction measurements due to the non-isokinetic sampling for volume ice fractions, $\Phi_v > 6.0\%$. A comparison between the calorimeter and batch measurements indicated the error in the local ice fraction measurements to be approximately in the order of $\pm 10\%$ for $\Phi_v > 6\%$.

Typical ice fraction profiles (Φ/Φ_m values) are plotted against the distance from the brass wall to the center of the sampling probe (y/H) in Fig. 10 for different mean volume ice fractions, Φ_v, up to 16%. Here, Φ_m represents the average value of the local ice fraction measurements. A small variation was observed in the ice fraction distribution across the flow channel, with local peaking near adiabatic walls. Similar wall peaking in volume fraction profiles of the dispersed phase have been previously reported to occur in vertical bubbly flows [35] as well as in the higher density sand–water flows [19]. However, at high volume ice fractions, $\Phi_v > 10\%$, the ice fraction distribution became flatter (see Fig. 10(b)). This flattening may be attributed to several factors such as the increase in the drag force exerted on the ice crystals and greater interactions between adjacent ice crystals at higher ice fraction ranges [19,34].

5. Conclusions

Local distribution measurements of the axial velocity and ice fraction were performed for the vertically, upward ice slurry flow in a 0.305-m (W) × 0.61-m (L) × 0.025-m (gap) rectangular channel with a channel aspect ratio of 1:12 under adiabatic flow conditions. A hot-film anemometer (HFA) and new ice slurry sampling technique were used to obtain the local distribution data. The measurements were conducted for volume ice fractions from 0% to 16%, and the mean bulk velocities of 0.10 and 0.15 m s^{-1}, respectively. The effects of the average volume ice fraction and Reynolds number ($Re_{cf} = 2000$–4000) on these distributions were explored. From the results, the following conclusions can be given.

1. The local ice velocity distribution measurements displayed flat profiles for average ice fractions as low as 2% by volume. The ice crystals were shown to produce a blunt velocity profile that deviates significantly from the profile measured in single-phase brine flows. For mean volume fractions less than 2%, the HFA results suggested that ice slurries behave similar to a single-phase flow.
2. For the range of velocities and volume ice fractions investigated, the effect of Reynolds number on the ice slurry velocity distribution was not very significant. Close examinations of the turbulence intensities indicated that the turbulent velocity fluctuations do not appreciably increase when the Reynolds number changed from 2200 to 4000, suggesting that the ice slurry flow retained its laminar character.
3. The local ice fraction distribution measurements systematically displayed peaking behavior near adiabatic walls for mean volume ice fractions less than 8%. At higher mean ice fractions ($\Phi_v > 10\%$), however, the local peaking near the walls disappeared and the ice fraction distributions became flatter.
4. The current local distribution measurements suggested that ice slurries displayed non-Newtonian flow characteristics for the ice fraction range from 2% to 9% and bulk mean velocities of 0.10 and 0.15 m s^{-1}. The present velocity data indicate that the non-Newtonian flow characteristics of ice slurries cannot be generally limited to high ice fractions as previously reported by others.

Acknowledgement

This project was financially supported by a CRD grant from the Natural Sciences and Engineering Research Council of Canada. The authors also would like to thank Sunwell Engineering Technologies for partially funding this project and the use of their space and facilities. The financial support from the Government of Ontario through the OGS-ST Scholarship for E.S. is also gratefully acknowledged.

References

[1] E. Choi, Y.I. Cho, H.G. Lorsch, Forced convection heat transfer with phase-change-material slurries: turbulent flow in a circular tube, Int. J. Heat Mass Transfer 37 (2) (1994) 207–215.

[2] P. Charunyakorn, S. Sengupta, S.K. Roy, Forced convection heat transfer in microencapsulated phase change material slurries: flow in circular ducts, Int. J. Heat Mass Transfer 34 (3) (1991) 819–833.
[3] Y. Yamagishi, H.T. Takeuchi, A.T. Pyatenko, N. Kayukawa, Characteristics of microencapsulated PCM slurry as a heat-transfer fluid, AIChE J. 45 (4) (1999) 696–707.
[4] V. Ayel, O. Lottin, H. Peerhossaini, Rhelogy, flow behavior and heat transfer characteristics of ice slurries: a review of the state of the art, Int. J. Refrig. 26 (2003) 95–107.
[5] J. Bellas, I. Chaer, S.A. Tassou, Heat transfer and pressure drop of ice slurries in plate heat exchangers, Appl. Therm. Eng. 22 (2002) 721–732.
[6] B.D. Knodel, D.M. France, U.S. Choi, M.W. Wambsganss, Heat transfer in ice–water slurries, Appl. Therm. Eng. 20 (2000) 671–685.
[7] C.A. Shook, M.C. Rocco, Slurry Flow: Principles and Practice Series in Chemical Engineering, Butterworth-Heinemann, Boston, 1991, pp. 27–33.
[8] G.B. Wallis, One Dimensional Two Phase Flow, McGraw-Hill, New York, 1969.
[9] G.W. Govier, K. Aziz, in: The Flow of Complex Mixture in Pipes, Van Nostrand Reinhold Company, New York, 1972, pp. 312–316.
[10] T. Kawanami, S. Fukusako, M. Yamada, Cold heat removal characteristics from slurry ice as a new phase change material, in: Natural Working Fluids '98, IIR-Gustav Lorentzen Conference: Proceedings of the Conference of Commission B2 with B1, E1 and E2, Oslo, Norway, 1998, pp. 146–156.
[11] A. Horibe, H. Inaba, N. Haruki, Melting heat transfer of flowing ice slurry in a pipe, in: S. Fukusako (Ed.), Proceedings of the Fourth Workshop on Ice Slurries of IIF/IIR, Int. Inst. of Refrig., Osaka, Japan, 2001, pp. 145–152.
[12] P.W. Egolf, O. Sari, F. Meili, P. Moser, D. Vuarnoz, Heat transfer of ice slurries in pipes, in: P.W. Egolf, O. Sari (Eds.), Proceedings of the First Workshop on Ice Slurries of IIF/IIR, Int. Inst. of Refrig., Yverdon-les-Bains, Switzerland, 1999, pp. 106–123.
[13] O. Sari, D. Vuarnoz, F. Meili, Visualization of ice slurries and ice slurry flows, Proceedings of the Second Workshop on Ice Slurries of IIF/IIR, Int. Inst. of Refrig., Paris, France, 2000.
[14] M. Kawaji, E. Stamatiou, R. Hong, V. Goldstein, Ice-slurry flow and heat transfer characteristics in vertical rectangular channels and simulation of mixing in a storage tank, in: S. Fukusako (Ed.), Proceedings of the Fourth Workshop on Ice Slurries, Int. Inst. of Refrig., Osaka, Japan, 2001, pp. 153–164.
[15] E. Stamatiou, M. Kawaji, V. Goldstein, Ice fraction measurements in ice slurry flow through a vertical rectangular channel heated from one side, in: P.W. Egolf (Ed.), Proceedings of the Fifth Workshop on Ice Slurries, Int. Inst. of Refrig., Stockholm, Sweden, 2002.
[16] D. Vuarnoz, O. Sari, P.W. Egolf, H. Liardon, Ultrasonic velocity profiler UVP-XW for ice-slurry flow characterization, in: Third International Symposium on Ultrasonic Doppler Methods for Fluid Mechanics and Fluid Engineering, EPFL, Lausanne, Switzerland, 2002, pp. 91–96.
[17] A. Kitanovski, A. Poredos, Concentration distribution and viscosity of ice-slurry in heterogeneous flow, Int. J. Refrig. 25 (2002) 827–835.
[18] R. Darby, Hydrodynamics of slurries and suspensions, in: N.P. Cheremisssinoff (Ed.), Encyclopedia of Fluid Mechanics, Slurry Flow and Technology, 5 (2), Gulf Pub., Houston, 1986, pp. 49–91.
[19] H. Nasr-El-Din, C.A. Shook, M.N. Esmail, Isokinetic probe sampling from slurry pipelines, Can. J. Chem. Eng. 62 (1984) 179–185.
[20] E. Stamatiou, Experimental study of the ice slurry thermal-hydraulic characteristics in compact plate heat exchangers, PhD thesis, University of Toronto, Toronto, Ont., Canada, 2003.
[21] H.H. Bruun, in: Hot-wire Anemometry: Principles and Signal Analysis, Oxford University Press, Oxford, 1995, p. 114.
[22] X. Sun, S. Kim, T.R. Smith, M. Ishii, Local liquid velocity measurements in air–water bubbly flow, Exp. Fluids 33 (2002) 653–662.
[23] E.J. Wasp, P.J. Kenny, R.L. Gandhi, Solid–Liquid Flow Slurry Pipeline Transportation, Gulf Publishing Co., Houston, 1979.
[24] J. Guilpart, L. Fournaison, B.M.A. Lakhdar, Calculation method of ice slurries thermophysical properties—application to water/ethanol mixture, in: 20th International Congress of Refrigeration, Sydney, 1999.
[25] D.G. Thomas, Transport characteristics of suspension: VIII. A note on the viscosity of Newtonian suspensions of uniform spherical particles, J. Coll. Sci. 20 (1965) 267–277.
[26] J.P. Hartnett, M. Kostic, Heat transfer to newtonian and non-newtonian fluids in rectangular ducts, in: J.P. Hartnett, T.F. Irvine Jr., (Eds.), Advances in Heat Transfer, vol. 19, 1989, pp. 247–356.
[27] M.S. Bhatti, R.K. Shah, Turbulent and transition flow convective heat transfer in duct, in: S. Kakac, R.K. Shah, W. Aung (Eds.), Handbook of Single-phase Convective Heat Transfer, John-Wiley and Sons, New York, 1987, pp. 4–7 (Chapter 4).
[28] M.A. Ben Lakhdar, J. Guilpart, A. Lallemand, Experimental study and calculation method of heat transfer coefficient when using ice slurries as secondary refrigerant CEMAGREF division GPAN Antony France, Heat and Technology (Pisa) 17 (2) (1999) 48–55.
[29] A.D. Maude, R.L. Whitmore, The wall effect and the viscometry of suspensions, Brit. J. Appl. Phys. 7 (1956) 98–102.
[30] M. Han, C. Kim, M. Kim, S. Lee, Particle migration in tube flow of suspensions, J. Rheol. 43 (5) (1999) 1157–1174.
[31] P.R. Nott, J.F. Brady, Pressure driven flow of suspensions: simulation and theory, J. Fluid Mech. 275 (1994) 157–199.
[32] J.-P. Matas, J.F. Morris, E. Guazzelli, Transition to turbulence in particulate pipe flow, Phys. Rev. Lett. 90 (1) (2003), Paper no. 014501-1.
[33] R.E. Hampton, A.A. Mammoli, A.L. Graham, N. Tetlow, S.A. Altobelli, Migration of particles undergoing pressure-

driven flow in a circular conduit, J. Rheol. 41 (3) (1997) 621–640.
[34] H. Nasr-El-Din, C.A. Shook, M.N. Esmail, Wall sampling in slurry systems, Can. J. Chem. Eng. 63 (1985) 746–753.
[35] G. Class, R. Meyder, W. Sengpiel, Measurements of spatial gas distribution and turbulence structure in developing bubbly two-phase flow in vertical channels, in: Proceedings of International Conference on Multi Flows '91, Tsukuba, Japan, 1, 1991, pp. 473–477.